Bioconjugate Chemistry

Article

pubs.acs.org/bc

Functionalization of Small Rigid Platforms with Cyclic RGD Peptides for Targeting Tumors Overexpressing $\alpha_v\beta_3$-Integrins

Jessica Morlieras,[†] Sandrine Dufort,[‡,§] Lucie Sancey,[†] Charles Truillet,[†] Anna Mignot,[†,‡,∥] Fabien Rossetti,[†] Mario Dentamaro,[†,⊥] Sophie Laurent,[⊥] Luce Vander Elst,[⊥] Robert N. Muller,[⊥] Rodolphe Antoine,[#] Philippe Dugourd,[#] Stéphane Roux,[¶] Pascal Perriat,[▲] François Lux,*[,†] Jean-Luc Coll,[§] and Olivier Tillement[†]

[†]Laboratoire de Physico-Chimie des Matériaux Luminescents, UMR 5620 CNRS − Université Claude Bernard Lyon 1, 69622 Villeurbanne Cedex, France

[‡]Nano-H SAS, 38070 Saint-Quentin Fallavier, France

[§]INSERM, CRI, U823, Institut Albert Bonniot, 38042 Grenoble, France

[∥]Matériaux, Ingénierie et Sciences, INSA Lyon, UMR 5510 CNRS − Université de Lyon, 69621 Villeurbanne Cedex, France

[⊥]NMR & Molecular Imaging Laboratory, Department of General Organic & Biomedical Chemistry, University of Mons, B-7000 Mons, Belgium

[#]Laboratoire de Spectrométrie Ionique et Moléculaire, UMR 5579 CNRS − Université Claude Bernard Lyon 1, 69622 Villeurbanne Cedex, France

[¶]Institut UTINAM, UMR 6213 CNRS-UFC, Université de Franche-Comté, 16 route de Gray, 25030 Besançon cedex, France

[▲]Matériaux, Ingénierie et Science, UMR 5510 CNRS-INSA de Lyon, 7 Avenue Jean Capelle, 69621 Villeurbanne Cedex, France

Supporting Information

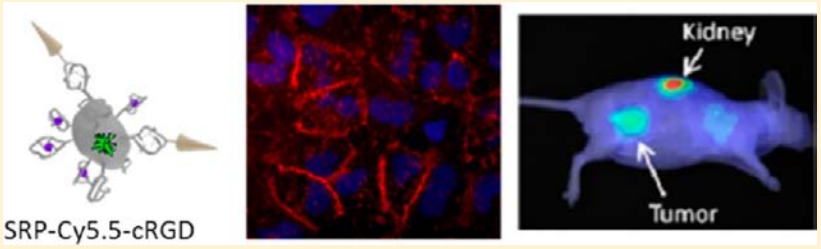

ABSTRACT: Gadolinium based Small Rigid Plaforms (SRPs) have previously demonstrated their efficiency for multimodal imaging and radiosensitization. Since the RGD sequence is well-known to be highly selective for $\alpha_v\beta_3$ integrins, a cyclic pentapeptide containing the RGD motif (cRGDfK) has been grafted onto the SRP surface. An appropriate protocol led to the grafting of two targeting ligands per nano-object. The resulting nanoparticles have demonstrated a strong association with $\alpha_v\beta_3$ integrins in comparison with cRADfK grafted SRPs as negative control. Flow cytometry and fluorescence microscopy have also been used to highlight the ability of the nanoparticles to target efficiently HEK293(β3) and U87MG cells. Finally the grafted radiosensitizing nanoparticles were intravenously injected into *Nude* mice bearing subcutaneous U87MG tumors and the signal observed by optical imaging was twice as high for SRP-cRGDfK compared to their negative analogue.

INTRODUCTION

One of the main challenges in the cancer nanomedicine field is the targeted delivery of nanoparticles to solid tumors for *in vivo* molecular imaging and targeted therapy.[1−5] Tumor targeting can be achieved by either passive or active process. Passive targeting takes advantage of the unique structural features of solid tumors, i.e., a hyperpermeable vasculature and an impaired lymphatic drainage.[6,7] Thereby, this enhanced permeability and retention (EPR) effect facilitates the efficient localization of long-term circulating nanoparticles within the tumor interstitium, but cannot promote their uptake by cancer cells. Afterward, active targeting approaches have been developed. They are based on the specific interactions between the ligands engrafted on the surface of nanoparticles and the overexpressed receptors on cancer cells and/or on microenvironment cells. This active process may promote internalization of nanoparticles through specific receptor-mediated endocytosis.[8−10]

Among the biomarkers that are currently being investigated for tumor targeting, the $\alpha_v\beta_3$ integrin is of particular interest.[11] $\alpha_v\beta_3$ integrins are overexpressed in sprouting vessels and also in 25% of human cancer cells of different types (glioblastoma, melanoma, prostate, breast, ovarian cancer),[11−15] and play a

Received: May 3, 2013
Revised: August 11, 2013
Published: August 26, 2013

dx.doi.org/10.1021/bc4002097 | Bioconjugate Chem. 2013, 24, 1584−1597

critical role in regulating tumor growth, metastasis, and angiogenesis.[16] The RGD sequence, an arginine-glycine-aspartic acid tripeptide, has been found to be highly selective for $\alpha_v\beta_3$ integrins,[17,18] and its cyclic form cRGDfK designed from the peptides developed by Kessler's group provides easy conjugation useful for imaging and/or therapeutic purposes.[17−19] Furthermore, many studies have demonstrated that a multivalent presentation of RGD peptides can significantly improve the binding affinity toward $\alpha_v\beta_3$ integrins and enhance tumor targeting capability.[20,21] For these reasons, many research groups have designed multivalent RGD nanoparticle conjugates for a variety of imaging applications, including magnetic resonance imaging (MRI),[22,23] positron emission tomography (PET),[24] single photon emission computed tomography (SPECT),[25] ultrasound imaging,[26] and optical imaging.[27,28] Recently, RGD-targeted nanoparticles have also been successfully employed for tumor drug delivery (chemotherapeutic drugs, nucleic acids)[29−32] and photothermal therapy.[33]

In this context, we have developed "theranostic" small rigid particles (SRPs), obtained *via* an original top down process (see Supporting Information Figure 1). They are composed of a polysiloxane matrix bearing chelating species, e.g., DOTA (1,4,7,10-tetraazacyclododecane-1,4,7,10-tetraacetic acid) at the surface. In a previous study, these nanoparticles have been validated as promising multimodal contrast agents used for four complementary imaging techniques, i.e., MRI, SPECT, CT, and optical imaging.[34] This is due to the DOTA ligands of which a fraction chelates Gd^{3+} ions allowing MRI, while another part remains free for radionuclide complexation (e.g., ^{111}In) to perform SPECT. Moreover, primary amine functions readily enable dye covalent conjugation to the polysiloxane matrix for fluorescence imaging studies. In addition, these gadolinium-based nanoparticles exhibit high radiosensitizing properties that render them hopeful therapeutic agents for radiotherapy.[35,36]

They ensure rapid renal clearance thanks to their small size after administration by intravenous injection or by the airways (<5 nm).[34,38] Despite a rapid clearance from the bloodstream, the amount of circulating nanoparticles is sufficient to observe by MRI a significant accumulation in tumor tissues, due to the EPR effect.[39] It is expected that this passive targeting combined with an active targeting, as that caused by the presence of the RGD motif onto the SRPs, should provide a more efficient accumulation of these particles in the tumor region.

Precisely, we aim to demonstrate that SRPs can be functionalized by peptides, such as cyclic RGDfK, while keeping their functionality and targeting effect both *in vitro* and *in vivo*. The targeting of cRGDfK functionalized SRPs was assessed by comparison with their nonbinding counterpart cRADfK functionalized SRPs. cRADfk is an analogue of cRGDfk where the glycine residue is changed into alanine. The physical and chemical properties (surface, size...) of the particles are only very slightly changed by the addition of this negative control that lost with this mutation its affinity for $\alpha_v\beta_3$[40] due to a conformational change in the peptide. The cyclic peptides were engrafted to SRPs with the method used for grafting cyanine 5.5:carbodiimide chemistry. Qualitative and quantitative characterizations were used to evaluate the number of grafted peptides per SRP, i.e., NMRD, PCS, FCS, ζ potential, MS, IR, UV−visible absorption, fluorescence spectroscopy, HPLC, and elemental analysis. The evaluation of biological properties of cRGDfK functionalized SRPs was first performed using FCS and IC_{50} tests. Then, cellular uptake was evaluated on different cell lines expressing $\alpha_v\beta_3$ integrins by flow cytometry and fluorescent microscopy. Finally, the fluorescently labeled SRPs-cRGDfK were injected intravenously in *Nude* mice bearing subcutaneous U87-MG tumors. Our work demonstrates that SRPs can be functionalized with cRGDfK peptides to obtain an efficient and active tumor targeting, both *in vitro* and *in vivo* in comparison with the negative controls (i.e., SRPs grafted with cRADfK peptides).

MATERIAL AND METHODS

Synthesis and Characterization of Targeting Particles.

Chemicals. *N*-(3-Dimethylaminopropyl)-*N*′-ethylcarbodiimide hydrochloride (EDC, >98.0%), *N*-hydroxysuccinimide (NHS, >97.0%), gadolinium chloride hexahydrate ($[GdCl_3.6H_2O]$, 99%), sodium hydroxide (NaOH, 99.99%), hydrochloric acid (HCl, 36.5−38%), sodium chloride (NaCl, >99.5%), dimethyl sulfoxide (DMSO, >99.5%), acetonitrile (CH_3CN, >99.9%), and trifluoroacetic acid (TFA, >99%) were purchased from Aldrich Chemical (France) and used without further purification. Preactivated Cyanine 5.5, later abbreviated Cy5.5-NHS, was purchased from GE Healthcare. The cyclic RGDfK and RADfK peptides were purchased from GeneCust (Luxembourg). The SRP synthesis has already been described elsewhere.[34] The core shell nanoparticles (core, gadolinium oxide; and shell, polysiloxane) and the SRPs were purchased from Nano-H SAS (Saint-Quentin Fallavier, France). The DOTAGA (1,4,7,10-tetraazacyclododecane-1-glutaric anhydride-4,7,10-triacetic acid) chelate was purchased from ChemaTech (Dijon, France). For preparation of an aqueous solution of nanoparticles, only milli-Q water (ρ > 18 MΩ.cm) was used.

Each synthesis step was performed at room temperature. SRP concentrations are stated in mol/L of gadolinium element.

Grafting of Cy5.5 on SRPs. Cy5.5-NHS was diluted in anhydrous DMSO (2.5 mg/mL) and added to an aqueous solution of SRPs (100 mM) at pH 7−7.4 for 8 h (molar ratio Cy5.5/Gd 0.044:1). Exclusively SRP-Cy5.5 allotted to cRGDfK or cRADfK grafting was submitted to tangential filtration to a 100 factor over a 5 kDa membrane before being treated by EDC and NHS activation reagents. This intermediate step remained necessary to remove any unconjugated dye and to avoid any future possible covalent conjugation between Cy5.5-NHS and cyclic RGDfK or RADfK peptides.

Activation of Carboxylic Acids from DOTA Molecules. For synthesis without Cy5.5, SRPs were dispersed in water 15 min before being added to EDC and NHS. The previous SRP and SRP-Cy5.5 solutions were treated by EDC and NHS at pH 5 for 30 min (molar ratio EDC/NHS/Gd 3:3:1).

Grafting of cRGDfK Peptide on SRPs. The previously activated SRP solutions, i.e., SRP and SRP-Cy5.5, were divided into three aliquots: one to be grafted with cyclic RGDfK peptide, another one to be grafted with cyclic RADfK peptide, and the last one to be used as a reference. At the same time, both cyclic RGDfK and RADfK peptides were dissolved in DMSO (100 mg/mL). Each peptide was mixed with one of the previously activated SRP aliquots at pH 7−7.4 for 8 h (molar ratio cPept./Gd 2:1). Similarly, the last sample considered as the reference was subjected to the same conditions, i.e., previously remaining activated SRP aliquot was mixed with DMSO at pH 7−7.4 for 8 h.

Addition of Gd^{3+} Ions. To achieve higher proton longitudinal relaxivities, additional Gd^{3+} ions were inserted into each SRP solution by adding a 100 mM Gd^{3+} solution

dx.doi.org/10.1021/bc4002097 | Bioconjugate Chem. 2013, 24, 1584−1597

prepared with $GdCl_3 \cdot 6H_2O$ in water (additional Gd^{3+}/initial Gd molar ratio 0.5:1). The final mixture was stirred for 6 h at pH 5−6.

Purification and Storage. Each SRP aliquot (i.e., SRP, SRP-cRGDfK, SRP-cRADfK, SRP-Cy5.5, SRP-Cy5.5-cRGDfK, and SRP-Cy5.5-cRADfK) was subjected to tangential filtration to a 1000 factor over a 5 kDa membrane to remove any unconjugated product and was freeze−dried for storage, using a Christ Alpha 1−2 lyophilizer. The freeze−dried SRPs are stable for months without alteration.

Phosphorescence Spectra for Free DOTA Quantification. Phosphorescence measurements were carried out using a Varian Cary Eclipse fluorescence spectrophotometer, with the time-resolved phosphorescence mode. Samples were pipetted into disposable glass-walled cells. Excitation slit was set to 20 nm, while emission slit was set to 10 nm. The spectra were recorded with an excitation wavelength of 395 nm and emission wavelengths from 550 to 650 nm. The photomultiplier tube (PMT) voltage was set to 800 V. The following parameters were used: delay time for data collection 100 μs and gate time 5 ms.

Size Measurement and Surface Potential. Hydrodynamic diameters (HD) and ζ-potentials of our samples were determined with a Zetasizer NanoS PCS (Photon Correlation Spectroscopy, laser He−Ne 633 nm) from Malvern Instruments. For HD measurements, 200 μL of an aqueous solution of SRPs (10 mM) was pipetted into a disposable microcuvette (ZEN0040). Attenuator and position were optimized by the device. Prior to ζ-potential experiments, the SRPs (10 mM) were diluted in an aqueous solution containing 0.01 M NaCl and adjusted to the desired pH. ζ-Potential measurements were recorded at 25 °C with palladium electrodes within a high concentration cell (ZEN1010). The ζ-potential was automatically calculated from electrophoretic mobility based on the Smoluchowski equation, $\nu = (\varepsilon E/\eta)\zeta$, where ν is the measured electrophoretic velocity, η is the viscosity, ε is the electrical permittivity of the electrolytic solution, and E is the electric field.

FCS (fluorescence correlation spectroscopy) study was performed as previously described[45] on the ConfoCor 2 system (Carl Zeiss, Jena, Germany) using a 40× water immersion C-Apochromat objective lens (numerical aperture (N.A.) = 1.2). The measurements were carried out at room temperature in 8-well Lab-Tek I chambered coverglass (Nalge Nunc International, Illkirch, France). The 633 nm He−Ne laser beam was focused into 50 μL solutions at 150 μm over the cover glass. The fluorescence emission was collected through a pinhole and a 650 nm long pass filter. Photon counts were detected by an Avalanche PhotoDiode at 20 MHz for 30 s. For each sample, FCS measurements were repeated 10 times. The data evaluation was performed using the Zeiss FCS Fit software (Zeiss, Jena, Germany).

Inductively Coupled Plasma − Optical Emission Spectroscopy (ICP-OES) Analysis. The determination of the accurate concentration of gadolinium in SRP samples was performed by ICP-OES with a Varian 710-ES spectrometer. First, SRPs were predispersed in water (100 mM). Small amounts of SRP aqueous solutions were diluted and heated at 80 °C for 3 h in 5 mL of concentrated nitric acid (67% HNO_3 (w/w)). Subsequently, the samples were scattered in 50 mL of water. For the calibration of the ICP-OES, single element standard solution was used and prepared from 1000 ppm Gd-standard from SCP Science by successive dilutions with an HNO_3 5% (w/w) matrix.

Mass Measurement. Full scan mass experiments were performed using a linear quadrupole ion trap mass spectrometer (LTQ, Thermo Fisher Scientific, San Jose, CA) with enlargement for the high 400−4000 Th range. The nanoparticle solution was electrosprayed at a flow rate of 5 μg/min in positive ion mode. Isotopic distributions of fragment ions were recorded using the zoom scan mode of the LTQ quadrupole ion trap mass spectrometer.

Infrared (IR) Spectra. The IR spectra of solid dry SRP samples were acquired on an IRAffinity-1, Shimadzu with an ATR platform by applying the attenuated total reflection Fourier transform infrared (ATR-FTIR) spectroscopy from 600 to 4000 cm^{-1}.

Nuclear Magnetic Relaxation Dispersion (NMRD) Profile. NMRD profiles extending from 0.12 mT to 1.2 T were recorded on a fast field cycling relaxometer (Stellar, Mede, Italy) on 0.8 mL solutions contained in 10-mm-o.d. tubes at 37 °C. Proton relaxation rates were also measured at 0.47 and 1.5 T with Minispec mq-20 and mq-60 (Bruker, Karlsruhe, Germany).

Ultraviolet−Visible Absorption Spectra. Aqueous solutions of SRPs were analyzed by UV−vis spectrophotometer (Varian Cary50) in the range of 200 to 800 nm, with a Hellma semimicro cell, 10 mm light path, 1400 μL, manufactured from Suprasil quartz.

Fluorescence Spectra for cRGDfK Quantification. Fluorescence measurements were carried out on an F-2500 Hitachi fluorescence spectrophotometer (Xe lamp). For all measurements, excitation and emission slits were set to 2.5 nm. The spectra were recorded with a final excitation wavelength of 240 nm and emission wavelengths from 240 to 310 nm. The photomultiplier tube (PMT) voltage was set to 700 V.

High Performance Liquid Chromatography. Gradient HPLC analysis was carried out using the Shimadzu Prominence series UFLC system equipped with a CBM-20A controller bus module, an LC-20AD liquid chromatograph, a CTO-20A column oven, an SPD-20A UV−visible detector, and an RF-20A fluorescence detector. Sample UV−visible absorption and fluorescence emission were respectively measured at 295 nm (UV−visible absorption single wavelength detection), 281 nm (λ_{exc} = 240 nm), and 692 nm (λ_{exc} = 590 nm) (simultaneous monitoring of two fluorescence emission wavelengths). Sample aliquots of 20 μL were loaded in 95% solvent A/5% solvent B (A = Milli-Q water/TFA 99.9:0.1 v/v ; B = CH_3CN/Milli Q water/TFA 90:9.9:0.1 v/v/v) onto a Jupiter C4 column (150 × 4.60 mm, 5 μm, 300 Å, Phenomenex) at a flow rate of 1 mL/min over 5 min. In a second step, samples were eluted by a gradient developed from 5% to 90% of solvent B in solvent A over 30 min. The concentration of solvent B was maintained over 10 min. Then, the concentration of solvent B was decreased to 5% over a period of 10 min to re-equilibrate the system, followed by additional 10 min at this final concentration. Before each sample measurement, a baseline was performed following the same conditions by loading Milli-Q water into the injection loop.

***In Vitro* Characterization of Targeting Properties.** *Cell Lines and Culture Conditions.* HEK293(β3) cells, stable transfectants of human β_3 subunit from the human embryonic kidney 293 cell line, were kindly supplied by J.-F. Gourvest (Aventis, France). They were cultured in DMEM (PAA, Linz, Austria), enriched with 4.5 g·L^{-1} glucose, 1% glutamine, and

dx.doi.org/10.1021/bc4002097 | *Bioconjugate Chem.* 2013, 24, 1584−1597

supplemented with 10% FBS, 700 μg.mL^{-1} G418 (G418 sulfate, PAA, Linz, Austria). U87MG cells, human radioresistant gliosarcoma cell line, were cultured in DMEM supplemented with 10% FBS and 1× nonessential amino acids. Cells were maintained at 37 °C in a humidified atmosphere of 5% CO_2. All the cells used here are integrin $\alpha_v\beta_3$-positive.

Association for Integrin $\alpha_v\beta_3$ by FCS Measurement. FCS equipment is described above. Most of the intensity autocorrelation curves were fitted using a free diffusion model with two components: the nanoparticle coupled to the fluorochrome alone and the fluorescent nanoparticle−integrin complex. Interaction assays were performed at RT in HBSS containing Mg^{2+} and Ca^{2+}. Soluble integrin $\alpha_v\beta_3$ (0.2 nmol, #CC1021, Chemicon) was mixed with SRP-cRGD-fK or SRP-cRAD-fK coupled to cyanine 5.5. FCS measurements were performed 5 min and 1 h after mixing. Preliminary studies enabled us to fix the diffusion time value of the first component and structural parameter. Moreover, a calibration step with 4 nmol/L Cy5 made it possible to evaluate the size of the confocal volume (≈1 μm^3).

Competitive Cell Adhesion Assays − IC_{50} Assay. Competitive assay was performed as described in Garanger et al., 2006.[45−47] Briefly, 96-well assay plates (Falcon, Becton Dickinson, France) were coated for 1 h at room temperature with 5 μg.mL^{-1} vitronectin in PBS and blocked for 30 min with 3% bovine serum albumin (BSA). Varying amounts of peptides were added simultaneously with 10^5 trypsinated HEK293(β3) cells to the wells and the plate was incubated for 30 min at 37 °C. Wells were rinsed three times with cold PBS to remove vitronectin-unbound cells. Attached cells were then fixed with absolute ethanol, stained with methylene blue, and quantified by OD reading at 630 nm. The activity of peptides was expressed as IC_{50} values (concentration of peptide necessary to inhibit 50% of cell attachment to the vitronectin substrate) and determinates from triplicates in three separate experiments.

Fluorescence Microscopy Analysis of SRP-Cy5.5-cPept Incubated in the Presence of Integrin $\alpha_v\beta_3$-Positive Cells. HEK293(β3) cells were grown on coverslips overnight at 37 °C, rinsed once with PBS, then with PBS containing 1 mM $CaCl_2$ and 1 mM $MgCl_2$. They were then incubated for 15 min at 4 °C (binding analysis) or 30 min at 37 °C (internalization analysis) in the presence of either SRP-Cy5.5, SRP-Cy5.5-cRGDfK, or SRP-Cy5.5-cRADfK at a concentration of 0.1 mmol.L^{-1} in Gd. They were subsequently rinsed with PBS Mg^{2+}/Ca^{2+} (1 mM) and fixed (10 min with 0.5% paraformaldehyde). Nuclei were labeled with Hoechst 33342 (Sigma Aldrich, Saint Quentin Fallavier, France) (5 μM) during 10 min. After being rinsed with PBS, coverslips were mounted in Mowiol. Fluorescence microscopy was performed on Apotome (Carl Zeiss, Jena, Germany).

Flow Cytometry Analysis of SRP-Cy5.5-cPept Incubated in the Presence of Integrin $\alpha_v\beta_3$-Positive Cells. For binding analysis, adherent cells were resuspended with trypsine, washed once with cold PBS, and another time with PBS containing 1 mM $CaCl_2$ and 1 mM $MgCl_2$. One million cells in a final volume of 200 μL were resuspended in SRP-Cy5.5-cPept suspensions (0.1 mmol.L^{-1} in Gd) in PBS Mg^{2+}/Ca^{2+} (1 mM) and incubated 15 min at 4 °C. SRP-Cy5.5-cPept solutions were removed and pellets carefully rinsed twice with PBS Mg^{2+}/Ca^{2+} (1 mM) at 4 °C. Cells were then rapidly analyzed by flow cytometry (LSRII, Becton Dickinson, France). The results were reported as Cy5.5 fluorescence histogram counts. For internalization analysis, the same experiment was performed with reagents at 37 °C, and the SRP-Cy5.5-cPept suspensions were incubated at 37 °C during 30 min.

***In Vivo* Characterization of Targeting Properties.** *In Vivo Fluorescence Imaging.* Female NMRI *Nude* mice (6 weeks old, Janvier, Le Genest Saint Isle, France) received a subcutaneous xenograft of U87MG cells (5×10^6 per mouse). After tumor growth, mice (n = 3 per group) were anesthetized (isoflurane/oxygen 4%/3.5% for induction and 2% thereafter) and were injected intravenously in the tail vein with 200 μL of SRP-Cy5.5-cPept suspension ([$Gd3^+$]~10 mmol/L), then they were illuminated by 660 nm light-emitting diodes equipped with interference filters. Fluorescence images as well as black and white pictures were acquired by back-thinned CCD camera at −80 °C (ORCAII-BT-512G, Hamamatsu, Massy, France) fitted with high pass filter RG9 (Schott, Jena, Germany).[27,28] All animal experiments were done in accordance with protocols approved by the Ethical comity of Grenoble. After imaging, the mice were killed and dissected for imaging organs. Image display and analysis were performed using the Wasabi software (Hamamatsu, Massy, France). Semiquantitative data were obtained from the fluorescent images by drawing regions of interest (ROI) on each organ. The results of organ fluorescence quantifications were expressed as a number of relative light units (RLU) per pixel per unit of time exposure.

Statistical Analysis. Statistical analysis was performed using two-tailed nonparametric Mann−Whitney t test. Statistical significance was assigned for values of $p < 0.05$.

RESULTS AND DISCUSSION

Coupling of Cy5.5, cRGDfK, and cRADfK Peptides to SRPs. *Synthesis.* SRPs were synthesized according to a route carefully described in a previous study.[35,39] This pathway allows the formation of SRPs displaying an average 3 ± 0.1 nm hydrodynamic diameter (HD) and an average 8.5 ± 1.0 kDa molecular mass. The number of DOTA molecules per SRP was estimated at about ten.[34] These SRPs exhibit some available primary amine functions (from the polysiloxane network) as well as carboxylic acid functions (from free DOTA ligands) for the further grafting of organic molecules. To perform grafting on the carboxylic function, only "free" DOTA ligands (i.e., DOTA molecules that do not chelate any gadolinium ion) can be used. The number of available DOTA molecules for further peptide coupling was determined by fluorescence titration. Roughly, small amounts of Eu^{3+} ions were added to the nanoparticles for the chelation by the "free" DOTA ligands. After 2 days of stirring at pH 5 and at room temperature, the fluorescence of the europium is measured. These conditions ensure that the europium is quantitatively bound to free DOTA groups.[39] An increase of the luminescence intensity ($\lambda_{excitation}$ = 395 nm) at 593 and 615 nm was observed during the titration until a plateau is observed. The increase of the intensity is due to the luminescence of the chelated Eu^{3+} ions that is orders of magnitude higher than that of unchelated Eu^{3+} ions that is quenched by water molecules (see Supporting Information). Ratios of about 30% of DOTA ligands chelating a Gd^{3+} ion and 70% of "free" DOTA molecules were observed for the so-prepared SRPs.

Some SRP *in vivo* biodistribution and biological implementations require near-infrared fluorescence; therefore, when needed, a Cy5.5 dye was grafted onto the SRPs. Cy5.5-NHS was covalently conjugated to amine functions present within the polysiloxane network while cyclic RGDfK and RADfK peptides were covalently grafted to carboxylic acid functions

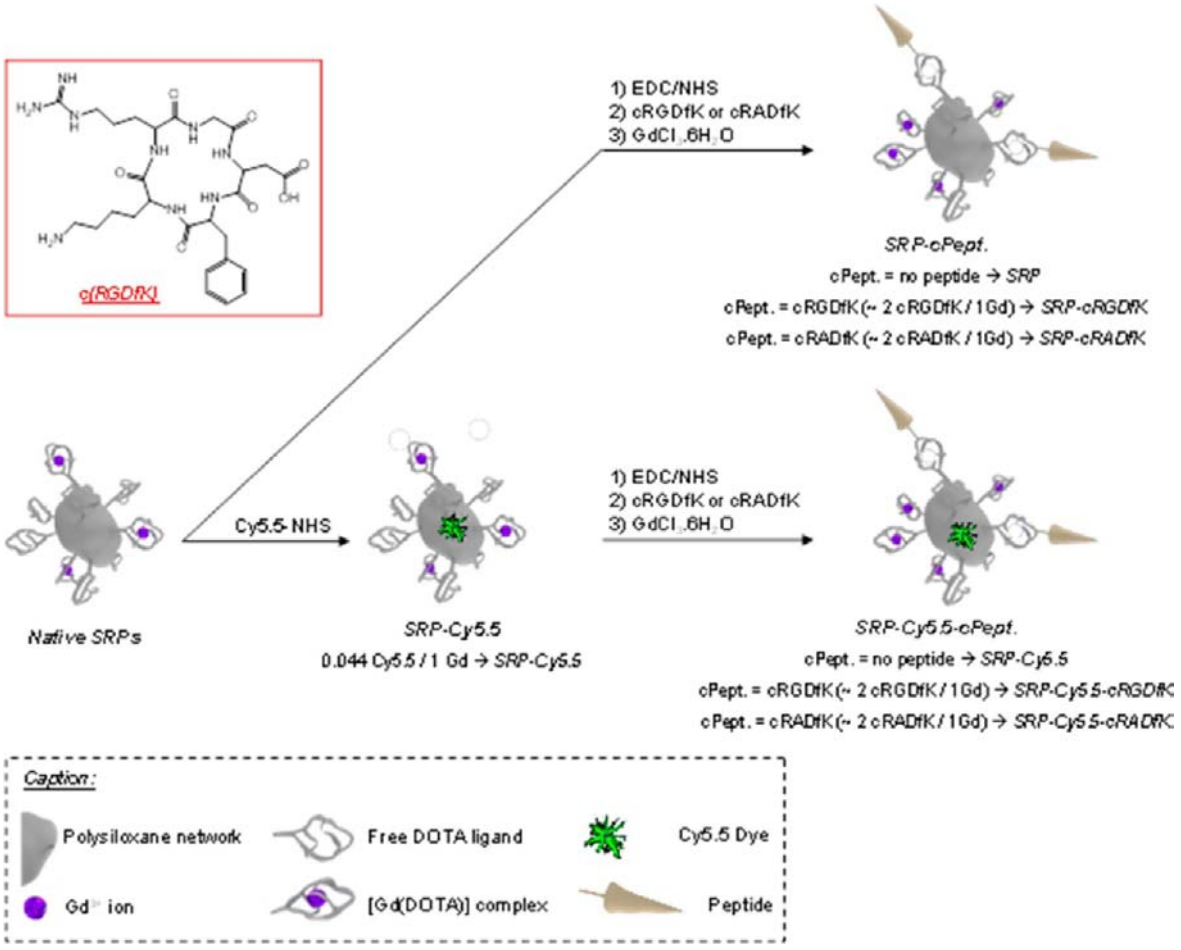

Figure 1. Scheme of Cy5.5 and cRGDfK (or cRADfK) peptide grafting reactions to SRPs and cRGDfK molecule design.

from free DOTA molecules *via* the amine function of the Lysine (see Figure 1). The carboxylic acid functions were activated by EDC/NHS before peptide addition.

Characterization of Grafted SRPs. The coupling of cRGDfK on the nanoparticles led to an increase of the hydrodynamic diameter (HD increases from 3.4 ± 0.5 nm for the native SRPs to 8.4 ± 0.5 nm for SRP-cRGDfK) (Figure 2(A)) These results were confirmed by FCS studies (Figure 2(C)) for Cy 5.5 bearing SRPs. By coupling the cyclic RGDfK peptide onto the SRP surface, a slightly higher surface charge is observed as expected in comparison with ungrafted SRPs (Figure 2(B)). This is due to the grafting of the cRGDfK that contains an amino function that is positively charged for pH inferior to 9. The presence of the cRGDfK was also confirmed by IR analysis (see Supporting Information) with the large increase of the 1500−1720 cm^{-1} band, that includes the 1654 cm^{-1} band generally assigned to amides (C═O stretching vibrations), the 1636 cm^{-1} band assigned to the guanidine group (C—N stretching vibrations),[41,42] and the 1598 cm^{-1} band assigned to primary amides (N—H bending vibrations).

Cyclic RGDfK peptide covalent conjugation to SRPs was also confirmed by mass spectrometry. For this, SRPs were first subjected to electrospray ionization (ESI) to generate ions in the gas phase and to obtain mass-to-charge information. As the SRPs contain ionized multiple groups (e.g., $[Gd^{III}(DOTA)]$ complexes), a distribution of charge states is often observed in the mass-to-charge spectrum. Those molecules can sustain multiple charges, which gives rise to an "envelope" of peaks in the spectrum.

A multiplicative correlation algorithm (MCA)[43] was used to estimate the mass of the SRPs from the mass-to-charge spectra produced by the ESI-MS (see Supporting Information). The main distribution for the SRP-cRGDfK particles was around 10.1 ± 0.4 kDa with a broader distribution at ~8.7 kDa. Charge states up to 8 were observed. This indicates that the carboxylic acid functions borne by the aspartic acid of the cyclic RGDfK peptide might decrease the number of negative charges of the SRP-cRGDfK compared to ungrafted SRPs in the positive mode. As a result, the charging capacity for functionalized SRPs with cRGDfK was, in this mode, higher than for the unfunctionalized SRPs in this mode.

The *m/z* 1217 peak in the positive mode of the ESI spectrum is characteristic of cRGDfK functionalized SRPs; its corresponding *m/z* 1215 peak in the negative mode was assigned to the $[Gd^{III}(DOTA\text{-}cRGDfK)(H_2O)]^-$ fragment, as evidenced by the isotopic distribution (see Figure 3). This result was confirmed by CID (collision-induced dissociation) analyses on this fragment (see Supporting Information). This *m/z* 1215 peak highlights the covalent conjugation of the cRGDfK peptide to the DOTA molecules *via* the primary amine side-chain group of the lysine. This conjugation only involves Gd^{3+} chelating DOTA since the free DOTA were conjugated to Gd^{3+} cations by addition of a gadolinium solution after the conjugation of the peptides in order to increase the r_1 of the SRPs.

dx.doi.org/10.1021/bc4002097 | *Bioconjugate Chem.* 2013, 24, 1584−1597

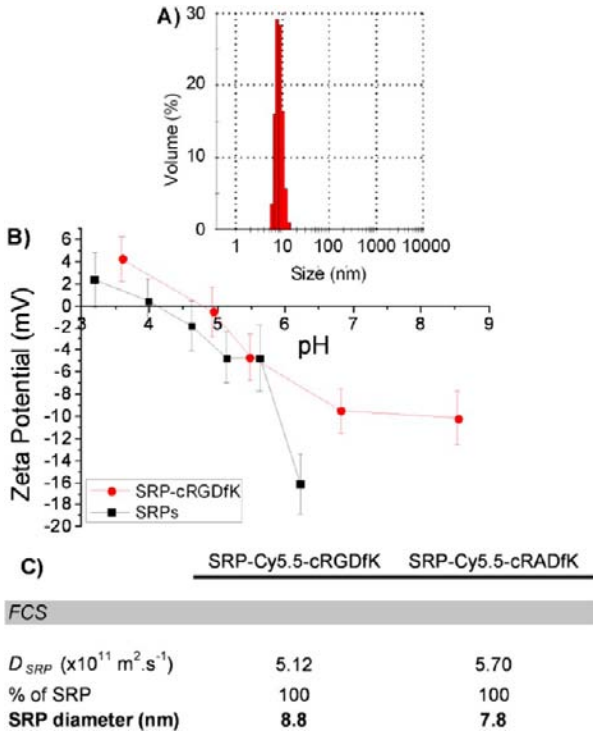

Figure 2. (A) SRP-cRGDfK PCS size measurements. (B) SRP-cRGDfK and SRP ζ-Potentials. (C) FCS analyses of SRP-Cy5.5-cRGDfK and SRP-Cy5.5-cRADfK at 633 nm. D is the diffusion coefficient.

Moreover, some details about the SRP structure had already been reported in earlier ESI-MS studies for low m/z ratios in the negative mode.[34] For example, it was noticed that the m/z 749 peak was specific to $[Gd^{III}(DOTA\text{-}Si(OH)_3)]^-$ fragment, namely, the $[Gd^{III}(DOTA)]^-$ complex borne by a silanetriol, belonging to the polysiloxane network (see Figure 3).

The negative charge was shared out by the four carboxylic acids from the DOTA molecule. As expected, this peak at m/z 749 was observed for both unfunctionalized and functionalized SRPs. An additional peak at m/z 630 was observed for both SRPs, matching an amide bond cleavage between DOTA and APTES molecules by loss of the $[NH(CH_2)_3Si(OH)_3]^-$ fragment.[40,41] This cleavage is accompanied by the creation of a C=C double bond, as the coordination number of Gd^{III} varies between 8 and 9, a water molecule addition in its coordination sphere (see Figure 3). Besides, the m/z 1215 fragment completely fits with the m/z 630 peak, adding the cRGDfK mass (603 Da) and removing the mass of a water molecule to allow the amide bond formation between the DOTA molecule and the peptide. This confirms again our conclusion upon the covalent conjugation of the cRGDfK peptide to the SRPs.

The proton longitudinal relaxation rates for SRP-cRGDfK were measured at 310 K, i.e., 37 °C, between 0.01 and 300 MHz on SRP-cRGDfK and compared with native SRPs and classical $[Gd^{III}(DOTA)(H_2O)]^-$ complexes. A higher relaxivity is observed for the cRGDfK functionalized SRPs in comparison with ungrafted SRPs regardless of the frequency used (see Figure 4). The increase of the longitudinal relaxivity is certainly due to an increase of the mass (due to the grafting of the peptide) and of the rigidity of the structure resulting in a slowdown of the rotation rate of the relaxing species.

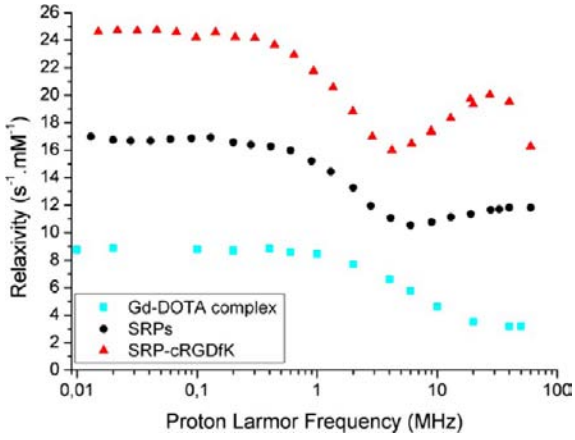

Figure 4. NMRD profiles of $[Gd^{III}(DOTA)(H_2O)]^-$ complex, SRPs, and SRP-cRGDfK.

Quantification of the Number of Peptides by Complementary Techniques. The quantification of the cRGDfK and Cy5.5 present in each particle has been obtained by

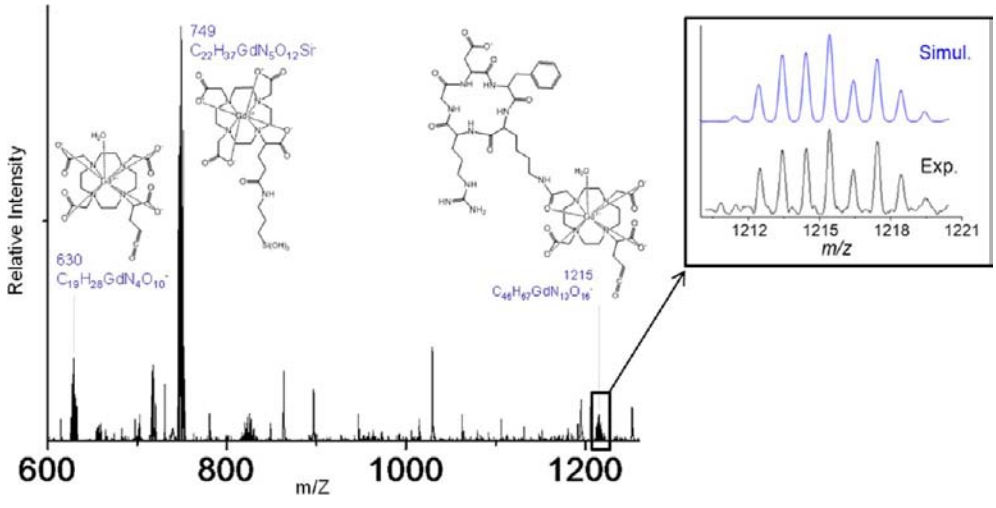

Figure 3. SRP-cRGDfK ESI spectra in a negative mode at low masses.

dx.doi.org/10.1021/bc4002097 | *Bioconjugate Chem.* 2013, 24, 1584−1597

complementary techniques. The UV−visible absorption spectrum of SRPs displays a specific intense peak at 295 nm and permits evaluation of the grafting of Cy5.5 thanks to its absorption peak at 680 nm after careful purification of all the ungrafted fluorophores. Evaluation of gadolinium was performed thanks to ICP-OES and validated by measurement of the longitudinal relaxivity at 60 MHz (see Table 1). cRGDfK

Table 1. Initial and Final Molar Dye/Gd and Dye/SRP Ratios and Percentage of Remaining Cy5.5 after Purification for SRP-Cy5.5-cPept

	Cy5.5 grafting yield	Final Cy5.5/Gd ratio	Final Cy5.5/SRP ratio
	UV−vis Absorption		
SRP-Cy5.5	89%	0.029	0.15
SRP-Cy5.5-cRGDfK	73%	0.049	0.25
SRP-Cy5.5-cRADfK	71%	0.047	0.24

displayed four non-intense specific peaks (ε < 100 L.mol^{-1}.cm^{-1}), from which three were thin and close together (λ = 252, 258, and 264 nm) and the remaining one was larger and flattened ($\lambda \sim$ 308 nm). Due to the overlap between the peaks characteristic of the peptide and those related to the particles, the UV−visible absorption spectra of the peptide grafted SRPs can only be used for a qualitative assessment of the coupling of cRGDfK on the nanoparticles, although the presence of the relatively intense absorption peak of the nanoparticles at 295 nm makes the quantification of the peptide impossible by this technique.

Fluorescence spectroscopy was then used to determine the peptide grafting rate. With the UV−visible excitation spectra of the peptide taken into account, the excitation wavelength was first set to 250 nm. However, the peptide fluorescence emission spectrum displayed a global signal, being the result of two contributions: water Raman and peptide emissions. To remove the contribution of the water Raman, whose spectral position depends on aqueous solution, on the excitation wavelength according to eq 1:[44]

$$\lambda_{\text{em water Raman peak (nm)}} = 10^7/[(10^7/\lambda_{\text{exc (nm)}}) - 3400] \quad (1)$$

the excitation wavelength was simply shifted by 10 to 240 nm (In the equation, $\lambda_{\text{em water Raman peak}}$ is the emission wavelength of the water Raman peak and λ_{exc} the excitation wavelength). This is sufficient to separate the two contributions, in order to solely observe the peptide fluorescence emission so avoiding gadolinium luminescence. To determine the quantity of peptide grafted per RGD, a standard fluorescence curve was plotted for different concentrations of peptide in the presence of the same amount of nanoparticles (see Figure 5). These spectra displayed two peaks: the widest and less intense, with a fluorescence maximum emission at 282 nm, was specifically assigned to the cyclic RGDfK peptide; its intensity varied linearly according to its concentration (Figure 5B). The other peak, with a fluorescence maximum emission at 261 nm, was attributed to water Raman; its intensity does not depend on the concentration of the peptide. Using such a calibration, a concentration of about 2 peptides per nanoparticle has been obtained (see Table 2).

Considering UV−visible absorption and emission fluorescence spectra, three specific wavelengths were selected to

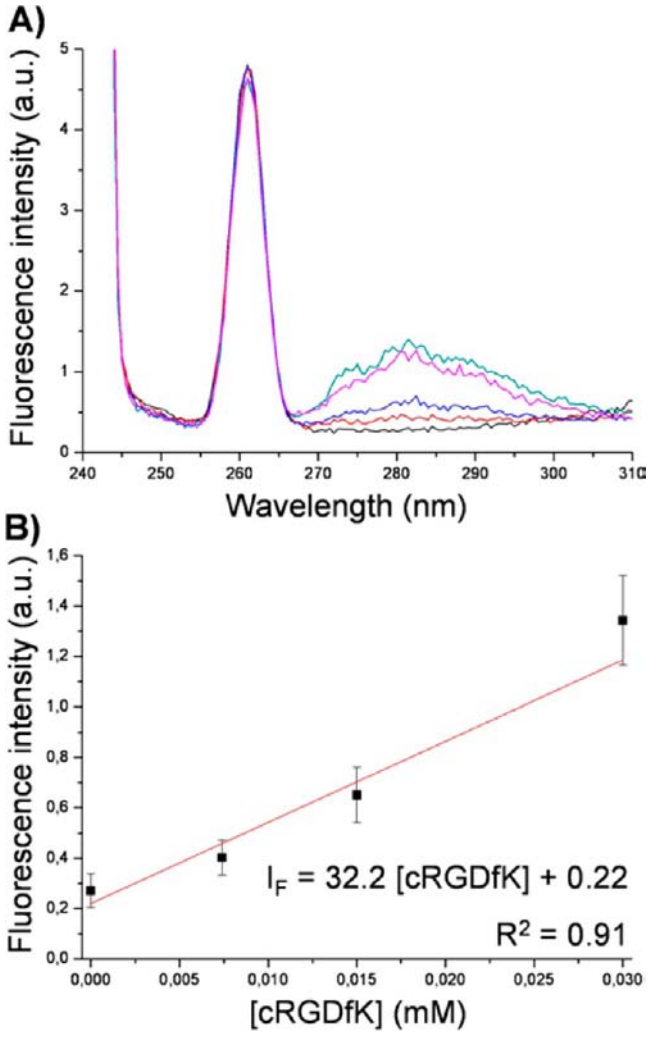

Figure 5. (A) Fluorescence Spectra of free cRGDfK in growing concentrations in presence of SRPs (constant concentration) for grafted cRGDfK determination (magenta, black, red, blue, dark cyan, and dark yellow lines). (B) cRGDfKmaxima fluorescence emission at λ_{em} = 282 nm versus the concentration of peptide added.

perform HPLC measurements. The UV−visible absorption detector wavelength was set to 295 nm; indeed, this wavelength is specific to SRPs and enabled the detection of SRP of any type (functionalized or not). Fluorescence emissions were simultaneously measured at two different wavelengths: 281 nm (λ_{exc} = 240 nm) and 692 nm (λ_{exc} = 590 nm) to observe the signals due to cRGDfK and Cy5.5, respectively. The samples were loaded into the injection loop and the corresponding chromatograms were collected after elution of a gradient of solvent (Figure 6(A), (B), and (C)).

The major signal proportion detected by UV−visible absorption at 295 nm was spotted at retention times ranging from 13 to 23 min. The smallest peak at 2.5 min was assigned to degradation fragments and remained negligible with respect to the previous signal. The experiment at 295 nm (Figure 6(A)) shows a shift of the peak from 13.7 min to higher retention times as a result of the grafting of peptides and/or cyanine. After Cy5.5 grafting, a certain proportion of the SRPs remains unfunctionalized since some particles are still detected corresponding to retention times around 13.7 min. The particles effectively functionalized by Cy5.5 are characterized

dx.doi.org/10.1021/bc4002097 | Bioconjugate Chem. 2013, 24, 1584−1597

Table 2. Final cRGDfK/SRP Molar Ratios Provided by Fluorescence Emission Spectra and by HPLC and Its Chromatograms Performed by Detection of Fluorescence Emission at 281 nm[a]

	SRPs	SRP-cRGDfK	SRP-Cy5.5	SRP-Cy5.5-cRGDfK
Fluorescence Emission (λ_{exc} = 240 nm, λ_{em} = 282 nm)				
Final cRGDfK/SRP ratio	/	**2.1**	/	**1.9**
HPLC (λ_{exc} = 240 nm, λ_{em} = 281 nm)				
Final cRGDfK/SRP ratio	/	**2**	/	**2.4**
Elemental Analysis				
Number of ... atoms/molecules per SRP				
Gd^{III}	5	5	5	5.5
DOTA	10	10	10	10
SiO_x	34.4	32.3	37.9	40.2
Cy5.5	/	/	0.15	0.27
cRGDfK	/	**2.5**	/	**2.2**

[a]Final cRGDfK/SRP ratios are also determined from elemental analysis assuming that each SRP displays 10 DOTA molecules and that the APTES/TEOS molar ratio remains constant during the purification steps.

by retention times around 15.2 min. On the contrary, after peptide grafting, all the particles are functionalized, the unique peak at 16 min being assigned to SRP-cRGDfK. These hypotheses were confirmed by fluorescence emission detections. With regard to the fluorescence emission recorded at 692 nm (λ_{exc} = 590 nm) (Figure 6(B)), the single peak observed were exclusively due to the conjugation of Cy5.5 to SRPs. SRP-Cy5.5 retention time was again centered around 15.2 min, while SRP-Cy5.5-cRGDfK retention time center was shifted to approximately 16.2 min which confirms the results obtained for the absorption at 295 nm (Figure 6(A)). Thanks to fluorescence emission recorded at 281 nm, the chromatogram of cyclic RGDfK was obtained and displays a retention time at 7.75 min. The chromatograms of the cRGDfK grafted SRPs displayed a short peak at this retention time being reminiscent of a very small proportion of unconjugated peptide, which is consistent with the conclusions drawn from Figure 6(A). However, the major proportion of the emission detected was collected at retention times ranging from 13 to 23 min. The cRGDfK chromatogram of Figure 6(C) is characterized by a linear relation between the area under the peak and the peptide concentration.[45] This is due to the absence of fluorescence for unfunctionalized SRPs at 281 nm. Chromatograms have been fitted with Gaussian curves. The related peptide concentrations calculated after a calibration similar to that performed in the case of fluorescent experiments are reported in Table 2.

A last evaluation of the peptide concentration was performed by elemental analysis taking into consideration the global mass of about 10 kDa determined by mass spectrometry (see Table 2). For this, two major hypotheses have been made: (1) like for the native nanoparticles, each SRP possesses 10 DOTA molecules; (2) the APTES/TEOS molar ratio of the polysiloxane network (60% APTES/40% TEOS) remains constant during the whole synthesis in particular during the purification steps. The molecular formulas were deduced with an absolute error ranging below 0.55% of the weight percentages supplied by elemental analyses (see Supporting Information).

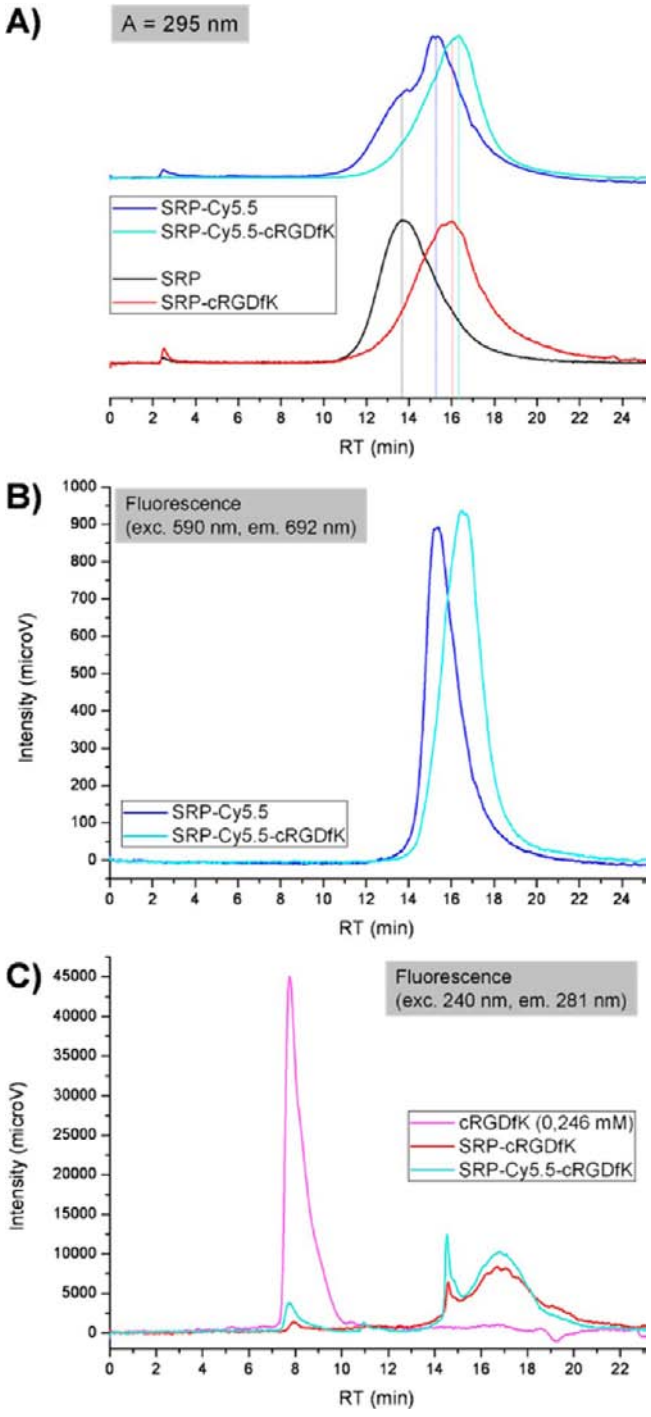

Figure 6. (A) Normalized chromatograms of SRP (black), SRP-cRGDfK (red), SRP-Cy5.5 (blue), and SRP-Cy5.5-cRGDfK (cyan) at UV−visible absorption wavelength = 295 nm. (B) Chromatograms of SRP-Cy5.5 (blue) and SRP-Cy5.5-cRGDfK (cyan) at fluorescence emission wavelength = 692 nm (λ_{exc} = 590 nm). (C) Chromatograms of cRGDfK (0.246 mM) (magenta), SRP-cRGDfK (red), and SRP-Cy5.5-cRGDfK (cyan) at fluorescence emission wavelength = 281 nm (λ_{exc} = 240 nm).

The numbers of cRGDfK per SRP deduced by elemental analysis are in good agreement with the values provided by fluorescence and HPLC. The average number of cRGDfK per SRP is between 1.9 and 2.5 for both SRP-cRGDfK and SRP-Cy5.5-cRGDfK. Since multimeric presentation of the RGD ligand is known to enhance $\alpha_v\beta_3$ integrin targeting,[46−48] the

dx.doi.org/10.1021/bc4002097 | Bioconjugate Chem. 2013, 24, 1584−1597

SRPs coupled to two cRGDfK are expected to demonstrate a high association with $\alpha_v\beta_3$ in *in vitro* binding assays and significant uptake in $\alpha_v\beta_3$-expressing tumors.

In Vitro Binding Assay. The targeting and the internalization of functionalized SRPs with cRGDfK were highlighted by several *in vitro* biological techniques: competitive assay (IC_{50} values), FCS (fluorescence correlation spectroscopy), fluorescence microscopy, and flow cytometry. The targeting of cRGDfK functionalized SRPs was systemically compared to the targeting of the nonbinding counterpart cRADfK functionalized SRPs and to the unfunctionalized SRPs as negative controls. For the last three *in vitro* techniques, i.e., FCS, fluorescence microscopy, and flow cytometry, the binding assays were performed on the fluorescently labeled SRPs: SRP-Cy5.5-cPept.

Association with $\alpha_v\beta_3$ Integrins. The diffusion properties of each fluorescently labeled SRP, i.e., SRP-Cy5.5-cRGDfK and SRP-Cy5.5-cRADfK, were first determined in solution using FCS. Then, an eventual modification of this parameter was measured in the presence of purified $\alpha_v\beta_3$ integrin. This should provide quantitative and qualitative information allowing the evidence of an association between the SRP-Cy5.5-cPept and the $\alpha_v\beta_3$ integrin. The diffusion coefficient *D* of the SRP-Cy5.5-cRGDfK, obtained by free diffusion model with 2 compartments, decreased strongly in the presence of the integrin, indicating the formation of complexes between the SRP-Cy5.5-cRGDfK and the integrin $\alpha_v\beta_3$. Precisely, we detected the presence of two different fluorescent species in the solution characterized by two different hydrodynamic diameters (HD) in the solution, a small one of 8.8 nm corresponding to the unbound SRP-Cy5.5-cRGDfK and the largest of 76.2 nm corresponding to the SRP-Cy5.5-cRGDfK/integrin complexes. To note, in this experiment we could not determine the number of integrin bound on the SRP-Cy5.5-cRGDfK. On the contrary, the diffusion coefficient *D* of the SRP-Cy5.5-cRADfK was not modified in the presence of the integrin, indicating as expected the total absence of interaction between the nonspecific SRP-Cy5.5-cRADfK and the integrin $\alpha_v\beta_3$. In other words, absolutely no complex was formed between the particle and the integrin. To resume, FCS analyses indicated that SRP-Cy5.5-cRGDfK were able to form a complex in the presence of the $\alpha_v\beta_3$ integrin in solution, whereas their nonbinding analogues (i.e., SRP-Cy5.5-cRADfK) cannot (see Table 3).

Table 3. FCS Analysis of the Interaction of Cy5.5 Labeled SRPs with Soluble $\alpha_v\beta_3$ Integrin at 633 nm[a]

	SRP-Cy5 5-cRGDfK + $\alpha_v\beta_3$ integrin	SRP-Cy5 5-cRADfK + $\alpha_v\beta_3$ integrin
FCS		
D_{SRP} ($\times 10^{11}$ m^2, s^{-1})	5.12	5.70
$D_{SRP\ with\ integrin}$($\times 10^{11}$ m^2,s^{-1})	0.584	NA
% of SRP	82.2	100
% of SRP with integrin	17.8	0
SRP diameter (nm)	8.3	7.8
SRP with integrin diameter (nm)	76.2	NA
Result	**Association**	**No association**

[a]The diffusion coefficients *D* of the SRPs being alone or in complex with the integrin are indicated. Only the SRP-Cy5.5-cRGDfK were able to complex with the integrin.

A competitive assay was also performed to evaluate deeper the binding of the cyclic RGDfK peptide grafted to SRPs. This competitive assay was expressed in terms of IC_{50} values (see Figure 7). Precisely, IC_{50} values evaluate SRP-cPept concentration necessary to inhibit 50% of some cell attachment to a vitronectin substrate. The vitronectin substrate is a substrate specific of the $\alpha_v\beta_3$ integrin and the cells chosen are HEK293(β3). The HEK293(β3) cell line was genetically modified to overexpress $\alpha_v\beta_3$ integrins, and is a great model to evaluate the RGD-dependent targeting *in vitro*.

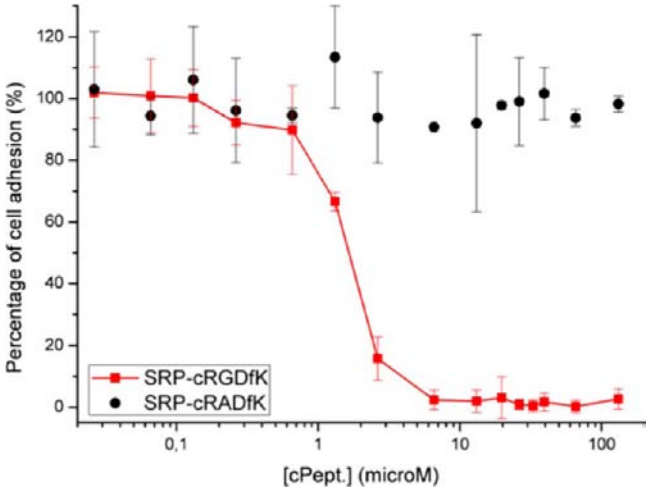

Figure 7. IC_{50} of SRP-cRGDfK and SRP-cRADfK on HEK293(β3) cells on vitronectin substrate. The IC_{50} curves depict a percentage of cell adhesion versus the concentration of the cyclic peptide.

Previous studies on regioselectively addressable functionalized template (RAFT) cyclodecapeptide scaffold bearing up to four cyclic RGDfK peptides have shown improved 10-fold association with $\alpha_v\beta_3$ integrin and an improved integrin-mediated internalization compared to the monomeric cyclic RGDfK peptide.[48,49] The same protocol of IC_{50} was used to perform the competitive binding assay on SRP-cRGDfK. The IC_{50} values of the RAFT scaffolds bearing 1, 2, 3, and 4 cyclic RGDfK peptides were respectively 48.8, 7.1, 2.8, and 4.1 μM. On Figure 7, the SRP-cRGDfK, which bore approximately 2.2 cRGDfK, possessed an efficient IC_{50} of 1.7 μM. This demonstrates a very high association of the SRP-cRGDfK with $\alpha_v\beta_3$ integrins equivalent to those of RAFT-RGD designed in the best conditions. As expected, their nonbinding counterparts, i.e., SRP-cRADfK, were not able to disrupt cell adhesion to vitronectin. The SRP-cRGDfK were evidenced to be promising candidates for $\alpha_v\beta_3$ integrin targeting.[48]

Association with Cells Expressing $\alpha_v\beta_3$ Integrins. The cellular uptake processes of SRP-Cy5.5, SRP-Cy5.5-cRGDfK, and SRP-Cy5.5-cRADfK were also assayed into HEK293(β3) cells by fluorescence microscopy and flow cytometry. The results obtained after incubation at 4 and 37 °C of SRP-Cy5.5-cPept (0.1 mmol/L in Gd) with HEK293(β3) cells are summarized in Figure 8. The incubation at 4 °C is suitable for studying specific targeting (Figure 8(A and B)), while the incubation at 37 °C allows SRP internalization (Figure 8(C and D)).

Fluorescence microscopy evidenced some specific HEK293(β3) targeting of SRP-Cy5.5-cRGDfK, in comparison with SRP-Cy5.5-cRADfK and SRP-Cy5.5 after 15 min of incubation at 4 °C. The SRP-Cy5.5-cRGDfK were observed on the surface

dx.doi.org/10.1021/bc4002097 | *Bioconjugate Chem.* 2013, 24, 1584−1597

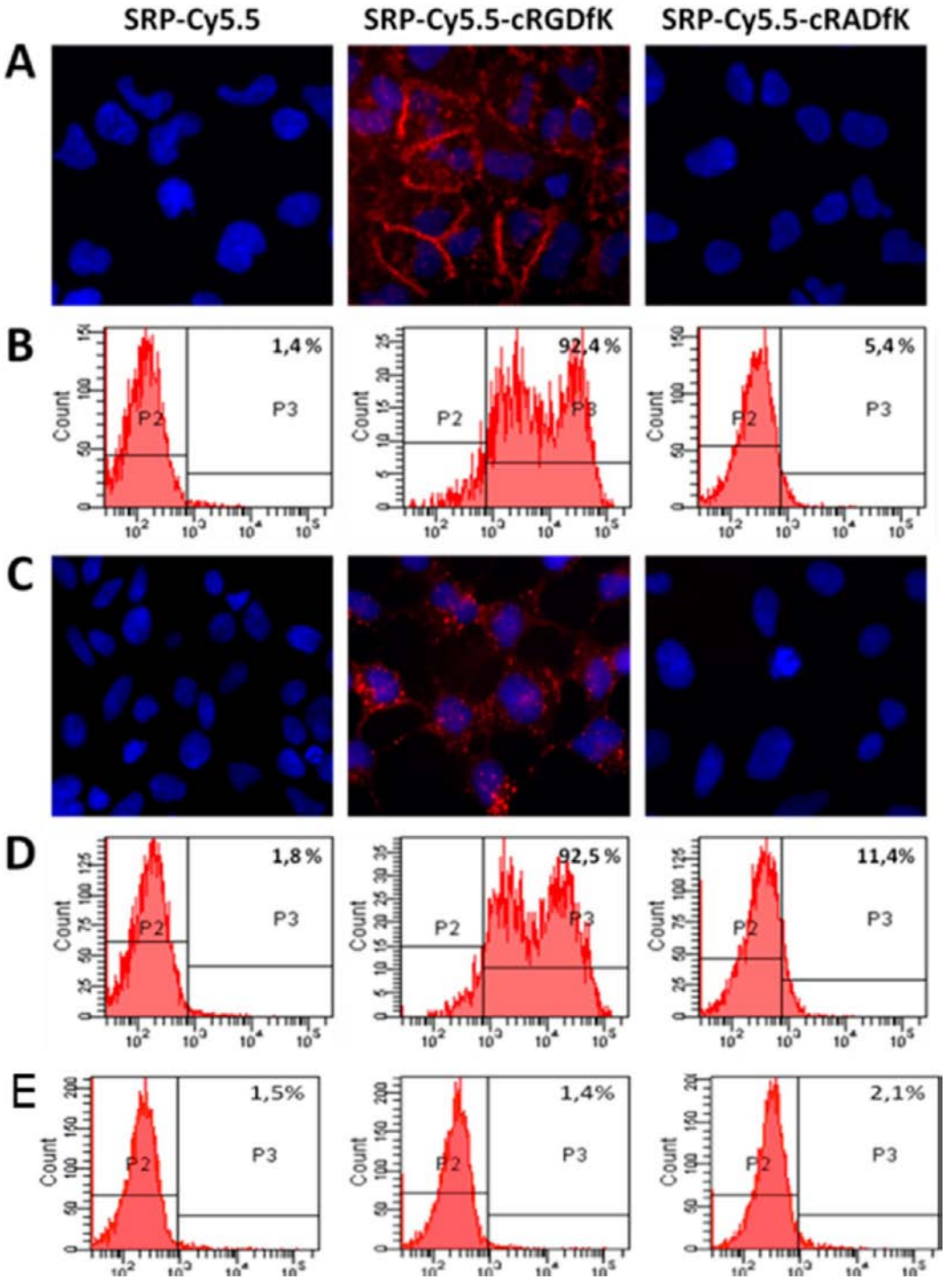

Figure 8. *In vitro* test of SRP-Cy5.5-cRGDfK, SRP-Cy5.5-cRADfK, and SRP-Cy5.5 in the presence of HEK293(β3) cells after 15 min incubation at 4 °C (A and B) or 30 min at 37 °C (C and D). Fluorescence microscopy pictures (A and C) and flow cytometry (B and D) evidenced the specific SRP-Cy5.5-cRGDfK (red) binding (A and B) and internalization (C and D), in comparison with the negative control SRP-Cy5.5-cRADfK and with SRP-Cy5.5. The cell nuclei were labeled in blue (Hoechst) on the fluorescence microscopy photographs (A and C). Red fluorescence is due to the Cy5.5 labeled nanoparticles. The figures on the flow cytometry plots (B and D) represent the percentages of labeled cells. *In vitro* evaluation of SRP-Cy5.5-cRGDfK, SRP-Cy5.5-cRADfK, and SRP-Cy5.5 interaction with HEK293(β1) cells after 30 min of incubation at 37 °C (E). Flow cytometry evidenced that there is no specific binding and internalization of SRP-Cy5.5-cRGDfK ($[Gd^{3+}] \sim 1$ mmol.L^{-1}).

of the cells and at cell junctions, where the $\alpha_v\beta_3$ integrins are likely to be overexpressed (Figure 8(A)). The specific interaction of HEK293(β3) with SRP-Cy5.5-cRGDfK led additionally to the internalization of some nanoparticles with an endosome-like pattern after 30 min of incubation at 37 °C, as evidenced by fluorescence microscopy (Figure 8(C)).

In all conditions, no SRP was observed inside the nucleus. These results were confirmed by flow cytometry analyses. Indeed, after incubations at 4 or 37 °C, the percentage of cells labeled by SRP-Cy5.5-cRGDfK was around 92% compared to 5−11% for SRP-Cy5.5-cRADfK or 2% for SRP-Cy5.5 (Figure 8(B and D)). The huge gap between the functionalized SRPs

dx.doi.org/10.1021/bc4002097 | *Bioconjugate Chem.* 2013, 24, 1584−1597

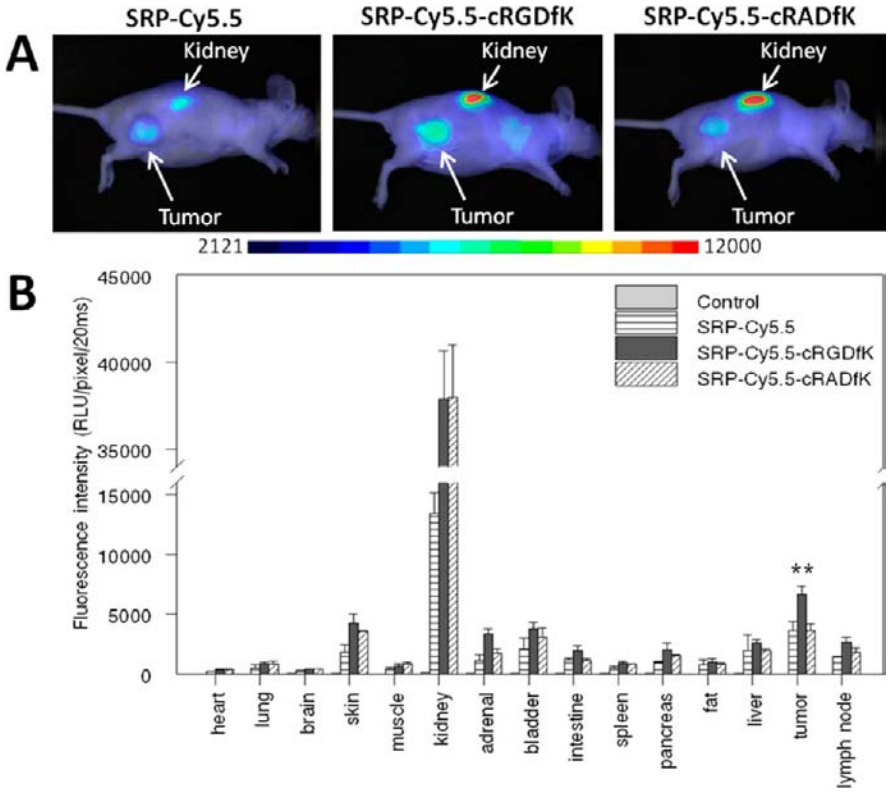

Figure 9. *In vivo* injection of SRP-Cy5.5, SRP-Cy5.5-cRGDfK, SRP-Cy5.5-cRADfK ($[Gd^{3+}] \sim 10$ mmol/L) in *Nude* mice carrying subcutaneous U87MG tumors. (A) Fluorescence images obtained 24 h after injection evidenced an accumulation of all particles in the tumor area, which was increased with SRP-Cy5.5-cRGDfK. Fluorescence images (20 ms integration time, color scale with contrast fixed between 2121 and 12000) were surimposed to visible light images (white and black). (B) Fluorescence images were then performed on isolated organs 24 h after injection, and ROIs were defined on the extracted organs in order to semiquantify the amount of photons detected per pixel after an exposure of 20 ms. Fluorescence is expressed in relative light unit per pixel per 20 ms. Controls were noninjected mice.

with cRGDfK and the functionalized SRPs with cRADfK or the unfunctionalized SRPs highlights again the specific interactions that exist between the SRP-Cy5.5-cRGDfK and the cells expressing $\alpha_v\beta_3$ integrins.

Similar experiments were also performed with cells expressing lower levels of $\alpha_v\beta_3$ integrin than HEK293(β3). For example, incubations of SRP-Cy5.5-cPept with U87MG cells provided similar results by flow cytometry analysis or fluorescence microscopy (see Supporting Information) than those obtained with HEK293(β3) cells.

In Vivo Targeting of SRP-Cy5.5-cPept. The targeting of the human radioresistant glioblastoma U87MG, expressing the $\alpha_v\beta_3$ integrin, presents a major interest. Indeed, glioblastoma is the most common form of primary brain tumor; its aggressive nature and evasiveness to conventional treatments make it one of the most lethal cancers. We have tested ungrafted SRPs on different HEK293(β3), TS/A-pc, and U87MG tumors to quantify the passive targeting of the particles on these models (see Supporting Information) due to the above-described enhanced permeability and retention effect. We observed that almost no passive targeting was observed for HEK293(β3) tumors probably due to the slow growth of the tumor. However, a minimum uptake by EPR effect is needed to observe an efficient active targeting, and this passive targeting was clearly visualized for U87MG and especially TS/A-pc tumors. However, in TS/A-pc tumors the expression of $\alpha_v\beta_3$ integrins is known to be very low, and the association of cRGDfK with these murine integrins is not as high as in the case of human integrins. To observe an efficient active targeting we have to search a model that simultaneously presents a strong passive accumulation of particles (i.e., a strong EPR effect) and an important expression of $\alpha_v\beta_3$ integrins with high association potential for cRGDfK. We then chose to evaluate the targeting ability of SRP-Cy5.5-cRGDfK in the case of the U87MG subcutaneous tumors that present the better compromise between an efficient EPR effect (to favor particles' entry) and a significant expression of $\alpha_v\beta_3$ integrins (to retain the particles entered).

The *in vivo* behavior of the SRP-Cy5.5-cPept was assessed following their intravenous injection in the tail vein of *Nude* mice bearing U87MG xenografts. The fluorescence imaging was performed at multiple time points after injection ($[Gd^{3+}] \sim 10$ mmol/L). Representative whole-body fluorescent images at 24 h after injection are shown in Figure 9.

The covalent conjugation of the cyclic RGDfK and RADfK peptides may not appear to modify drastically the biodistribution of the SRPs. These particles are small enough to pass through the renal filter and to be evacuated rapidly, thus avoiding damage and toxicity related to the long-term retention observed with larger ones. However, although our preliminary data suggest that there is no toxicity for the kidneys, this issue should be carefully evaluated (study in progress). Each SRP-Cy5.5, functionalized or not with peptides, presented a passive accumulation in tumors, due to the EPR effect. But, similarly to the *in vitro* results, a significant specific and active additional accumulation of SRP-Cy5.5-cRGDfK was observed in the tumor area. Indeed, the fluorescence intensities quantified on the remote tumors containing SRP-Cy5.5-cRGDfK are twice as

dx.doi.org/10.1021/bc4002097 | *Bioconjugate Chem.* 2013, 24, 1584−1597

high as in the case of the negative control SRP-Cy5.5-cRADfK ($p < 0.01$**) (Mann−Whitney U test was used to assess the significant level between independent variables. The level of significance was set to $p < 0.05$). This indicates the specific and active capability of SRP-Cy5.5-cRGDfK to target $\alpha_v\beta_3$ expressing tumors. These results are very interesting, because in all the previously published studies *in vivo* active targeting was never observed.[27,28] In the most favorable cases, the grafting of peptides (like cRGDfK or cRADfK) could increase tumor passive accumulation compared to unfunctionalized nanoparticles, but no difference between the targeting particles and their negative control could be detected.[27] On the contrary, the present results show that the grafting with the negative control (cRADfK) does not increase passive particle accumulation in tumors compared with unfunctionalized particles. Additional accumulation is only obtained using the targeted particles by cRGDfK which demonstrates unambiguously the presence of an active effect. The size and more generally the design of the SRPs developed here permit to get model particles that respond to the expected behavior of active particles.

CONCLUSIONS

The $\alpha_v\beta_3$ integrin is overexpressed on neoformed endothelial cells of the tumor vasculature and on many tumor cells. The RGD sequence is a highly selective ligand for the $\alpha_v\beta_3$ integrin and the natural recognition process of this RGD motif by the integrin is mediated by multivalent interactions. In this context, we aimed to develop multimeric RGD containing scaffolds. The SRPs were selected as the RGD carriers thanks to their interesting properties in terms of size, rigidity, detection, and radiosensitizing effects. First, and according to their small size, the SRPs ensure rapid renal clearance but they are sufficiently large to avoid extravasation from normal blood vessels and to display long circulation time in the bloodstream. Then, these SRPs enable multimodal imaging (MRI, SPECT, fluorescence imaging) and are very promising for radiotherapy.[34−36] The covalent grafting of RGD containing peptides on the SRP surface renders them hopeful for tumor selective diagnosis and for targeted therapy. To benefit from multivalent interaction of cRGDfK toward $\alpha_v\beta_3$ integrins, about 2 peptides have been grafted per particles. The *in vitro* $\alpha_v\beta_3$ integrin targeting of cRGDfK functionalized SRPs was evidenced directly toward $\alpha_v\beta_3$ integrins or cells known to express $\alpha_v\beta_3$ integrins such as HEK293(β3) and U87MG. The active targeting of these particles has been confirmed by complementary tests fusing cRADfK functionalized SRPs as negative control. Finally, *in vivo* tumor uptake was significantly highlighted using fluorescence imaging after intravenous injection of the fluorescently labeled SRPs functionalized with cRGDfK in *Nude* mice bearing U87MG tumors. U87MG tumors have been chosen because of the radiosensitizing properties of this type of particle against glioma tumors. We hope that this first *in vivo* active targeting proof for SRP on U87MG models will be particularly interesting for further radiotherapy guided by imaging experiments performed on glioblastoma.

ASSOCIATED CONTENT

Supporting Information

Synthesis of the SRPs; titration of free DOTA by fluorimetry; IR spectroscopy; UV-visible absorption; fluorescence spectroscopy; elemental analysis.This material is available free of charge via the Internet at http://pubs.acs.org.

AUTHOR INFORMATION

Corresponding Author

*E-mail: francois.lux@univ-lyon1.fr.

Author Contributions

Jessica Morlieras and Sandrine Dufort contributed equally to the work.

Notes

The authors declare no competing financial interests.

ACKNOWLEDGMENTS

We wish to thank the COST action TD1004 "theranostics imaging and therapy: an action to develop novel nanosized systems for imaging-guided drug delivery" and the COST action D38 "Metal-based systems for molecular imaging applications". M.D., S.L., L.V.E., and R.N.M thank the French Community of Belgium (ARC Programmes 95/00−194, 00/05−258 and 05/10−335), the Fond National de la Recherche Scientifique (FNRS), the support and concerted sponsorship of COST Action D38, the EMIL Programme and the Center for Microscopy and Molecular Imaging (CMMI), supported by the European Regional Development Fund and the Walloon Region. Thanks are also due to French programs ANR-12-RPIB-0010 Multimage and ANR-12-P2N-0009-Gd-Lung.

REFERENCES

(1) Cho, K., Wang, X., Nie, S., Chen, Z. G., and Shin, D. M. (2008) Therapeutic nanoparticles for drug delivery in cancer. *Clin. Cancer Res. 14*, 1310−1316.

(2) Davis, M. E., Chen, Z. G., and Shin, D. M. (2008) Nanoparticles Therapeutics: an emerging treatment modality for cancer. *Nat. Rev. Drug Discovery 7*, 771−782.

(3) Ferrari, M. (2005) Cancer nanotechnology. *Nat. Rev. Cancer 5*, 161−171.

(4) Jain, R. K., and Stylianopoulos, T. (2010) Delivering nanomedicine to solid tumors. *Nat. Rev. Clin. Oncol. 7*, 653−664.

(5) Riehemann, K., Schneider, S. W., Luger, T. A., Godin, B., Ferrari, M., and Fuchs, H. (2009) Nanomedicine-Challenge and Perspectives. *Angew. Chem., Int. Ed. Engl. 48*, 872−897.

(6) Hobbs, S. K., Monsky, W. L., Yuan, F., Roberts, W. G., Griffith, L., Torchilin, V., and Jain, R. K. (1998) Regulation of transport pathways in tumor vessels: role of tumor type and microenvironment. *Proc. Natl. Acad. Sci. U. S. A. 95*, 4607−4612.

(7) Matsumura, Y., and Maeda, H. (1986) A new concept for macromolecular therapeutics in cancer chemotherapy: mechanism of tumirotropic accumulation of proteins and the antitumor agent smancs. *Cancer Res. 46*, 6387−6392.

(8) Desgrosellier, J. S., and Cheresh, D. A. (2010) Integrins in cancer: biological implications and therapeutic opportunities. *Nat. Rev. Cancer 10*, 9−22.

(9) Kirpotin, D. B., Drummond, D. C., Shao, Y., Shalaby, M. R., Hong, K., Nielsen, U. B., Marks, J. D., Benz, C. C., and Park, J. W. (2006) Antibody targeting of long-circulating lipidic nanoparticles does not increase tumor localization but does increase internalization in animal models. *Cancer Res. 66*, 6732−6740.

(10) Park, J. W., Benz, C. C., and Martin, F. J. (2004) Future directions of liposome- and immunoliposome- based cancer therapeutics. *Semin. Oncol. 31*, 196−205.

(11) Beer, A. J., and Schwaiger, M. (2008) Imaging of integrin alphavbeta3 expression. *Cancer Metastasis Rev. 27*, 631−644.

(12) Beck, V., Herold, H., Benge, A., Luber, B., Hutzler, P., Tschesche, H., Kessler, H., Schmitt, M., Geppert, H. G., and Reuning, U. (2005) ADAM15 decreases integrin alphavbeta3/vitronectin-mediated ovarian cancer cell adhesion and mobility in an RGD-dependent fashion. *Int. J. Biochem. Cell Biol. 37*, 590−603.

(13) Chen, X., Liu, S., Hou, Y., Tohme, M., Park, R., Bading, J. R., and Conti, P. S. (2004) MicroPet imaging of breast cancer alphav-

integrin expression with 64Cu-labeled dimeric RGD peptides. *Mol. Imaging Biol. 6*, 350−359.
(14) Ding, Q., Stewart, J., Jr., Olman, M. A., Klobe, M. R., and Gladson, C. L. (2003) The pattern of enhancement of Src kinase activity on platelet-derived growth factor simulation of glioblastoma cells is affected by the integrin engaged. *J. Biol. Chem. 278*, 39882−39891.
(15) Kuphal, S., Bauer, R., and Bosserhoff, A. K. (2005) Integrin signaling in malignant melanoma. *Cancer Metastasis Rev. 24*, 195−222.
(16) Hood, J. D., and Cheresh, D. A. (2002) Role of integrins in cell invasion and migration. *Nat. Rev. Cancer 2*, 91−100.
(17) Dobrucki, L. W., de Muinck, E. D., Lindner, J. R., and Sinusas, A. J. (2010) Approaches to multimodality imaging of angiogenesis. *J. Nucl. Med. 1 51* (Suppl 1), 66S−79S.
(18) Temming, K., Schiffelers, R. M., Molema, G., and Kok, R. J. (2005) RGD-based strategies for selective delivery of therapeutics and imaging agents to the tumour vasculature. *Drug Resist. Update 8*, 381−402.
(19) Schottelius, M., Laufer, B., Kessler, H., and Wester, H. J. (2009) Ligands for mapping alphavbeta3-integrin expression in vitro. *Acc. Chem. Res. 42*, 969−980.
(20) Garanger, E., Boturyn, D., and Dumy, P. (2007) Tumor targetting with RGD peptide ligands-design of new molecular conjugates for imaging and therapy of cancer. *Anticancer Agents Med. Chem. 7*, 552−558.
(21) Liu, S. (2006) Radiolabeled multimeric cyclic RGD peptides as integrin alphavbeta3 targeted radiotracers for tumor imaging. *Mol. Pharmaceutics 3*, 472−487.
(22) Chen, K., Xie, J., Xu, H., Behera, D., Michalski, M. H., Biswal, S., Wang, A., and Chen, X. (2009) Triblock copolymer coated iron oxide nanoparticle conjugate for tumor integrin targeting. *Biomaterials 30*, 6912−6919.
(23) Zhang, F., Huang, X., Zhu, L., Guo, N., Niu, G., Swierczewska, M., Lee, S., Xu, H., Wang, A. Y., Mohamedali, K. A., Rosenblum, M. G., Lu, G., and Chen, X. (2012) Noninvasive monitoring of orthotopic glioblastoma therapy response using RGD-conjugated iron oxide nanoparticles. *Biomaterials 33*, 5414−5422.
(24) Wadas, T. J., Deng, H., Sprague, J. E., Zheleznyak, A., Weilbaecher, K. N., and Anderson, C. J. (2009) Targeting the alphavbeta3 integrin for small-animal PET/CT of osteolytic bone metastases. *J. Nucl. Med. 50*, 1873−1880.
(25) Haubner, R., and Decristoforo, C. (2009) Radiolabelled RGD peptides and peptidomimetics for tumour targeting. *Front. Biosci. 14*, 872−886.
(26) Borden, M. A., Zhang, H., Gillies, R. J., Dayton, P. A., and Ferrara, K. W. (2008) A stimulus-responsive contrast agent for ultrasound molecular imaging. *Biomaterials 29*, 597−606.
(27) Goutayer, M., Dufort, S., Josserand, V., Royere, A., Heinrich, E., Vinet, F., Bibette, J., Coll, J. L., and Texier, I. (2010) Tumor targeting of functionalized lipid nanoparticles: assessment by in vivo fluorescence imaging. *Eur. J. Pharm. Biopharm. 75*, 137−147.
(28) Yong, K. T., Hu, R., Roy, I., Ding, H., Vathy, L. A., Bergey, E. J., Mizuma, M., Maitra, A., and Prasad, P. N. (2009) Tumor targeting and imaging in live animals with functionalized semiconductor quantum rods. *ACS Appl. Mater. Interfaces 1*, 710−719.
(29) Borgman, M. P., Aras, O., Geyser-Stoops, S., Sausville, E. A., and Ghandehari, H. (2009) Biodistribution of HPMA copolymer-amino-hexylgeldanamycin-RGDfK conjugates for prostate cancer drug delivery. *Mol. Pharmaceutics 6*, 1836−1847.
(30) Han, H. D., Mangala, L. S., Lee, J. W., Shahzad, M. M., Kim, H. S., Shen, D., Nam, E. J., Mora, E. M., Stone, R. L., Lu, C., Lee, S. J., Roh, J. W., Nick, A. M., Lopez-Berestein, G., and Sood, A. K. (2010) Targeted gene silencing using RGD-labeled chitosan nanoparticles. *Clin. Cancer Res. 16*, 3910−3922.
(31) Jiang, J., Yang, S., Wang, J. C., Yang, L. J., Xu, Z. Z., Yang, T., Liu, X. Y., and Zhang, Q. (2010) Sequential treatment of drug-resistant tumors with RGD-modified liposomes containing Si-RNA or doxorubicin. *Eur. J. Pharm. Biopharm. 76*, 170−178.
(32) Zhan, C., Gu, B., Xie, C., Li, J., Liu, Y., and Lu, W. (2010) Cyclix RGD conjugated poly(ethylen glycol)-co-poly(lactic acid) micelle enhances paclitaxel anti-glioblastoma effect. *J. Controlled Release 143*, 136−142.
(33) Li, Z., Huang, P., Zhang, X., Lin, J., Yang, S., Liu, B., Gao, F., Xi, P., Ren, Q., and Cui, D. (2010) RGD-conjugated dendrimer-modified gold nanorods for in vivo tumor targeting and photothermal therapy. *Mol. Pharmaceutics 7*, 94−104.
(34) Lux, F., Mignot, A., Mowat, P., Louis, C., Dufort, S., Bernhard, C., Denat, F., Boschetti, F., Brunet, C., Antoine, R., Dugourd, P., Laurent, S., Vander Elst, L., Muller, R., Sancey, L., Josserand, V., Coll, J. L., Stupar, V., Barbier, E., Remy, C., Broisat, A., Ghezzi, C., Le Duc, G., Roux, S., Perriat, P., and Tillement, O. (2011) Ultrasmall rigid particles as multimodal probes for medical applications. *Angew. Chem., Int. Ed. Engl. 50*, 12299−12303.
(35) Le Duc, G., Miladi, I., Alric, C., Mowat, P., Brauer-Krisch, E., Bouchet, A., Khalil, E., Billotey, C., Janier, M., Lux, F., Epicier, T., Perriat, P., Roux, S., and Tillement, O. (2011) Toward an image-guided microbeam radiation therapy using gadolinium-based nanoparticles. *ACS Nano 5*, 9566−9574.
(36) Mowat, P., Mignot, A., Rima, W., Lux, F., Tillement, O., Roulin, C., Dutreix, M., Bechet, D., Huger, S., Humbert, L., Barberi-Heyob, M., Aloy, M. T., Armandy, E., Rodriguez-Lafrasse, C., Le Duc, G., Roux, S., and Perriat, P. (2011) In vitro radiosensitizing effects of ultrasmall gadolinium based particles on tumour cells. *J. Nanosci. Nanotechnol. 11*, 7833−7839.
(37) Choi, H. S., Liu, W., Liu, F., Nasr, K., Misra, P., Bawendi, M. G., and Frangioni, J. V. (2010) Design consideration for tumour-targeted nanoparticles. *Nat. Nanotechnol. 5*, 42−47.
(38) Bianchi, A., Lux, F., Tillement, O., and Crémillieux, Y. (2013) Contrast enhanced lung MRI in mice using ultra-short echo time radial imaging and intratracheally administrated Gd-DOTA-based nanoparticles. *Magn. Reson. Med.*, DOI: 10.1002/mrm.24580.
(39) Mignot, A., Truillet, C., Lux, F., Sancey, L., Louis, C., Denat, F., Boschetti, F., Bocher, L., Gloter, A., Stephan, O., Antoine, R., Dugourd, P., Luneau, D., Novitchi, G., Figueiredo, L. C., De Morais, P. C., Bonneviot, L., Albela, B., Ribot, F., Van Lokeren, L., Dechamps-Olivier, I., Chuburu, F., Lemercier, G., Villiers, C., Marche, P. N., Le Duc, G., Roux, S., Tillement, O., and Perriat, P. (2013) A top-down synthesis route to ultrasmall multifunctionnal Gd-based silica nanoparticles for theranostic applications. *Chem.—Eur. J. 19*, 6122−6139.
(40) Hijnen, N. M., de Vries, A., Nicolay, K., and Grüll, H. (2013) Dual-isotope ^{111}In/^{177}Lu SPECT imaging as a tool in molecular imaging tracer design. *Contrast Media Mol. Imaging 7*, 214−222.
(41) Braiman, M. S., Briercheck, D. M., and Kriger, K. M. (1999) Modeling vibrationnal spectra of amino acids in proteins. III. Effects of protonation state, Counterion, and solvent on arginine C-N stretch frequencies. *J. Phys. Chem. 103*, 4744−4750.
(42) Morales-Avila, E., Ferro-Flores, G., Ocampo-Garcia, B. E., De Leon-Rodriguez, L. M., Santos-Cuevas, C. L., Garcia-Becerra, R., Medina, L. A., and Gomez-Olivan, L. (2011) Multimeric system of 99m Tc-labeled gold nanoparticles to c[RGDfK(C)] for molecular imaging of tumor $\alpha(v)\beta(3)$ expression. *Bioconjugate Chem. 22*, 913−922.
(43) Hagen, J. J., and Monning, C. A. (1994) Method for estimating molecular mass from electrospray spectra. *Anal. Chem. 66*, 1877−1883.
(44) Lawaetz, A. J., and Stedmon, C. A. (2009) Fluorescence intensity calibration using the raman scatter peak of water. *Appl. Spectrosc. 63*, 936−940.
(45) Kafka, A. P., Rades, T., and McDowell, A. (2010) Rapid and specific high-performance liquid chromatography for the in vitro quantification of D-Lys6-GnRH in a microemulsion-type formulation in the presence of peptide oxidation products. *Biomed. Chromatogr. 24*, 132−139.
(46) Maheshwari, G., Brown, G., Lauffenburger, D. A., Wells, A., and Griffith, L. G. (2000) Cell adhesion and mobility depend on nanoscale RGD clustering. *J. Cell. Sci. 113*, 1677−1686.
(47) Mammen, M., Choi, S. K., and Whitesides, G. M. (1998) Polyvalent interactions in biological systems: implications for design

and use of multivalent ligands and inhibitors. *Angew. Chem., Int. Ed. Engl.* 37, 2754−2794.
(48) Galibert, M., Sancey, L., Renaudet, O., Coll, J. L., Dumy, P., and Boturyn, D. (2010) Application of click-click chemistry to the synthesis of new multivalent RGD conjugates. *Org. Biomol. Chem.* 8, 5133−5138.
(49) Sancey, L., Garanger, E., Foillard, S., Schoehn, G., Hurbin, A., Albiges-Rizo, C., Boturyn, D., Souchier, C., Grichine, A., Dumy, P., and Coll, J. L. (2009) Clustering and internalization of integrin alphavbeta3 with a tetrameric RGD-synthetic peptide. *Mol. Ther.* 17, 837−843.